Sensors and Materials, Vol. 37, No. 10 (2025) 4383–4402
MYU Tokyo

S & M 4188

Experimental Study of the Polarization Properties of Anodic Porous Alumina Membranes Embedded with Gold through Electrolysis

Masanori Nagata,[1] Singo Fukuoka,[1] Yu Oshiro,[2]
Isao Tsunoda,[2] and Toyonori Matsuda[2*]

[1]Kumabou Metal Co., Ltd., 1-4-15 Nagamine-West, Higashi-Ward, Kumamoto 861-8037, Japan
[2]National Institute of Technology, Kumamoto College, Kumamoto Campus
2659-2 Suya, Koshi, Kumamoto 861-1102, Japan

(Received July 16, 2025; accepted September 17, 2025)

Keywords: anodic porous alumina, Au nanoparticles, polarization, Stocks parameter, Fabry–Pérot interference, localized surface plasmons

An experimental study was conducted to investigate the polarization properties of the specularly reflected light from an anodic porous alumina (APA) membrane in which gold (Au) is embedded into the nanopores of APA by alternating current electrolysis. Consequently, we revealed that, when the Au-embedded APA membrane is considered to have the arrays of Au nanoparticles with rod-like shapes, the specularly reflected light changes rapidly from right- to left-circular polarization via linear polarization with respect to a slight variation in the angle of incidence of the incident light at a wavelength of 532 nm. The variation in the state of polarization, which is measured as a rapid change in the Stokes parameter s_3, can be attributed to the simultaneous occurrence of the Fabry–Pérot interference in the single layer of APA and the excitation of localized surface plasmons on Au rod-like nanoparticle arrays. The rapid change in s_3 has the potential to provide the effective information about the structural parameters of the Au-embedded APA membrane, such as the dimension of the Au rod-like nanoparticles or the refractive index of materials filling the nanopores of the APA layer.

1. Introduction

Anodic porous alumina (APA), which is formed by the anodization of aluminum (Al) in an acidic electrolyte, consists of regularly arrayed nanoscale cells of a hexagonal alumina cylinder with a pore at the center. APA has been the subject of extensive research, ranging from its sophisticated fabrication processes to advanced applications.[1,2] The fabrication of APA based on a two-step anodization process[3] allows for the formation of highly ordered arrays of nanopores with tunable structural parameters, e.g., pore diameter, pore spacing, and pore length.[1,4] APA has attracted considerable interest in a wide range of fields, including photonics[5] and sensors,[6] as porous materials with advanced features attributed to the presence

*Corresponding author: e-mail: tmatsu@kumamoto-nct.ac.jp
https://doi.org/10.18494/SAM5848

ISSN 0914-4935
https://myukk.org/

of highly ordered nanopore arrays[5] and as templates for the fabrication of a variety of nanostructured architectures such as nanowires and nanotubes.[7]

One of the optical devices utilizing the ordered nanopore arrays of APA is an APA membrane in which metal, such as gold (Au) or silver (Ag), is embedded into the nanopores.[8–12] The metal-embedded APA membrane has been studied for various applications, e.g., structural coloration,[13,14] optical sensors,[15–17] catalyst for nanowire synthesis,[18] and nanocomposite.[19] The metal-embedded APA membrane comprises an APA layer in which nanometer-sized metal particles (e.g., nanorods) are regularly arranged in a matrix on an Al substrate. Therefore, the Au- (or Ag-) embedded membrane has been investigated for the excitation of localized surface plasmons (LSPs)[20] on the regular arrays of Au (or Ag) nanorods.[9,10,12,14] Moreover, the metal-embedded APA membrane causes the Fabry–Pérot (FP) interference[5,21] where the incident light is multiply reflected at the top and bottom interfaces of the APA layer. Thus, the metal-embedded APA membrane induces the LSP excitation and FP interference, and their combined or synergistic effect leads to the achievement of the required optical properties.[13,16]

The metal-embedded APA membrane can be fabricated in a simple, cost-effective, and large-area manner by using electrochemical approaches: an anodization process[3] forms an APA layer on an Al plate and an electrolysis process[22,23] deposits metal into the nanopores of the APA layer. The structural parameters of the metal-embedded APA membrane, such as the shape and dimension of the deposited metal nanoparticles, are controlled by tuning the conditions of anodization and electrolysis processes.[8,22] The structural parameters have a significant effect on the optical characteristics of metal-embedded APA membranes, including the LSP resonance and/or the FP interference. Therefore, investigating the effects of the structural parameters on the optical characteristics is important for the achievement of the optical features required for metal-embedded APA membranes. The optical characteristics of metal-embedded APA membranes have been studied, but many of them deal with characteristics related to the intensity of the reflected or transmitted light.[8–10,12,13] It seems that the polarization properties of the reflected light from metal-embedded APA membranes have not yet been adequately investigated. Detailed studies into the polarization properties of metal-embedded APA membranes, particularly those related to the LSP resonance and FP interference, may lead to interesting polarization features attributed to the presence of the regular arrays of metal nanoparticles in the APA layer.

In this study, we discuss the polarization properties of the specular reflected light from Au-embedded APA membranes while relating them to the state of Au deposition within the APA layer. We prepared an APA membrane by two-step anodization, and we then deposited Au into the nanopores of the APA membrane in the electrolyte solution of gold compound by alternating current electrolysis.[23] The state of Au deposition within the Au-embedded membrane is tuned by electrolysis conditions,[8,10,13] such as electrolysis voltage, electrolysis duration, and the temperature of the electrolyte solution. We fabricated several Au-embedded APA membranes through the alternating current electrolysis at different voltages while keeping other electrolysis conditions constant. The Au-embedded APA membranes were used as samples where the state of Au deposition was tuned by the electrolysis voltage. The elemental depth-profiling analysis of the elements, O (oxygen), Al and Au, for the Au-embedded APA membranes with different

electrolysis voltages was performed through glow discharge-optical emission spectrometry (GD-OES) to examine the state of Au deposition inside the APA membrane.[24] The analysis results indicate that the state of Au deposition changes with an increase in electrolysis voltage. Particularly, when the electrolysis voltage is within a certain range, Au is deposited within the APA membrane in rod-like shapes, resulting in the formation of the arrays of Au rod-like nanoparticles. We investigated the polarization properties of the specularly reflected light from the Au-embedded APA membranes with the various states of Au deposition tuned by the electrolysis voltage: the wavelength of the incident light was set to 532 nm, which excites LSP on Au nanoparticles,[9,10] and the incident-angle dependence of the state of polarization was measured. As a result, we reveal that, when the Au-embedded APA membrane is considered to have the arrays of Au nanoparticles with rod-like shapes, the specularly reflected light rapidly and markedly changes the state of polarization with respect to a slight variation in the angle of incidence. This polarization property is measured as a rapid change in normalized Stokes parameter, which indicates the difference in intensity between the right- and left-circularly polarized components of the specularly reflected light. We examine the rapid change in s_3 by studying the phase difference and the amplitude ratio between the *p* and *s* components of the specularly reflected light. This suggests that the rapid change in s_3 is associated with the simultaneous occurrence of the FP interference in the APA layer and the LSP excitation on the regular arrays of Au rod-like nanoparticles. The occurrence of the FP interference and LSP excitation is highly dependent on the configuration of the Au-embedded APA membrane and its constituent materials. Therefore, the rapid change in s_3 expects to include the effective information about the structural parameters of the Au-embedded APA membrane, such as the dimension of Au rod-like nanoparticles and the refractive index of materials filling the nanopores of the APA layer. The rapid change in s_3 can be considered an attractive polarization property attributed to the Au nanoparticle arrays within the APA layer.

2. Fabrication of Au-embedded APA Membranes

Here, we describe the process of fabricating the Au-embedded APA membranes examined in this study. Two-step anodization accompanied by a process to promote the deposition of Au into the nanopores of APA[24–27] was employed to prepare an APA membrane. Alternating current electrolysis[23] was used to deposit Au into the nanopores of the APA membrane.

2.1 APA formation by two-step anodization

We used a pure Al plate (YAMAMOTO-MS Co., Ltd., 99.85% or more, 25 × 40 mm^2, 0.3 mm thick, Japan) as the substrate on which APA is formed by two-step anodization. Prior to anodization, the surface of the Al plate was cleaned by degreasing and alkaline etching. The cleaned Al plate was then anodized in 0.3 mol/dm^3 oxalic acid solution at 25 °C for 120 min by applying a constant DC voltage of 50 V, as first-step anodization. The (disordered) porous alumina formed in the first-step anodization was dissolved by immersion in a mixed aqueous solution of 2 wt% (mass percent concentration) chromic anhydride and 6 wt% phosphoric acid at

90 ℃ for 30 min. The porous-alumina-removed Al plate was again anodized under the same anodizing conditions as in the first-step anodization, but the anodization duration was set to 10 min. At the end of the second-step anodization, the process that the anodization current was reduced by half at 2.5 min intervals was repeated a total of five times. The reduction in anodization current is indicative of a concomitant reduction in anodic oxidation voltage, which follows an exponential decrease.

The (exponential) decrease in anodization voltage promotes the deposition of Au within the APA membrane by electrolysis.[24–27] The anodization process without the anodization voltage decrease for an Al plate forms a straight tubular nanopore layer and a barrier layer adjacent to the surface of the Al substrate. The barrier layer made of alumina provides corrosion resistance and insulation for the APA membrane. If the anodization voltage decrease process is carried out at the end of the second-step anodization, the bottom of the straight tubular nanopores then branches out to form dendritic structures[25–27] and the barrier layer becomes thinner.[24] Therefore, the anodization voltage decrease process provides conductive paths for Au ions in an electrolyte solution to reach the Al substrate, and thus promotes Au deposition within the dendritic nanopore region directly above the barrier layer during electrolysis.

2.2 Embedding of Au within APA by electrolysis

We embedded Au within the APA membrane prepared by the above anodization process by alternating current electrolysis.[23] We used an aqueous solution of tetrachloroauric acid ($HAuCl_4$, 1 g/dm^3) and sulphuric acid (H_2SO_4, 7 g/dm^3) as an electrolyte. The APA membrane was aged in the electrolyte solution at 30 °C for 5 min with stirring. An AC voltage E [V] of 60 Hz (e.g., 4.5 V) was then applied between the Al substrate of the APA membrane and the platinum-coated titanium mesh plate (opposite electrode) in the electrolyte solution at 30 ℃ for 10 min. The alternating current electrolysis facilitates the diffusion and migration of tetrachloroaurate ions ($AuCl_4^-$) near the surface of the Al substrate. The alternating current electrolysis assists the ionization of the tetrachloroaurate ions ($AuCl_4^- \rightarrow Au^{3+} + 4Cl^-$) and the reduction of Au^{3+} ions ($Au^{3+} + 3e^- \rightarrow Au$) on the working electrode (Al substrate), resulting in the Au deposition within the dendritic nanopore region in APA. Thus, we fabricated the Au-embedded APA membrane by alternating current electrolysis with the electrolysis voltage E.

Figure 1 shows a schematic illustration of a Au-embedded APA membrane and SEM images of its cross section. The Au-embedded APA membrane is formed from an APA layer and an Al substrate. The APA layer consists of a straight-tubular (nanopore) layer, a dendritic (nanopore) layer, and a barrier layer. We denote the diameter and spacing of the nanopores in the straight-tubular layer by D and P, respectively. Figure 1(b) shows the SEM image of the cross section of the Au-embedded APA membrane with E = 4.5 V. The Au-embedded APA membrane was scratched with a diamond cutter, cooled with liquid nitrogen, and then broken. The fractured surface was observed by SEM (Hitachi High-Tech, SU8600, Japan). The thickness of the straight-tubular layer is H_S = 5187 ± 103 nm and that of the dendritic layer including the barrier layer is H_D = 216 ± 16 nm from the SEM image. The thickness of the APA layer, $H_S + H_D \sim$ 5.4 μm, is close to the value of 6 μm measured using an eddy-current coating thickness gauge (Helmut Fischer GmbH, ISOSCOPE FMP10, Germany). As shown in Fig. 1(c), a dendritic

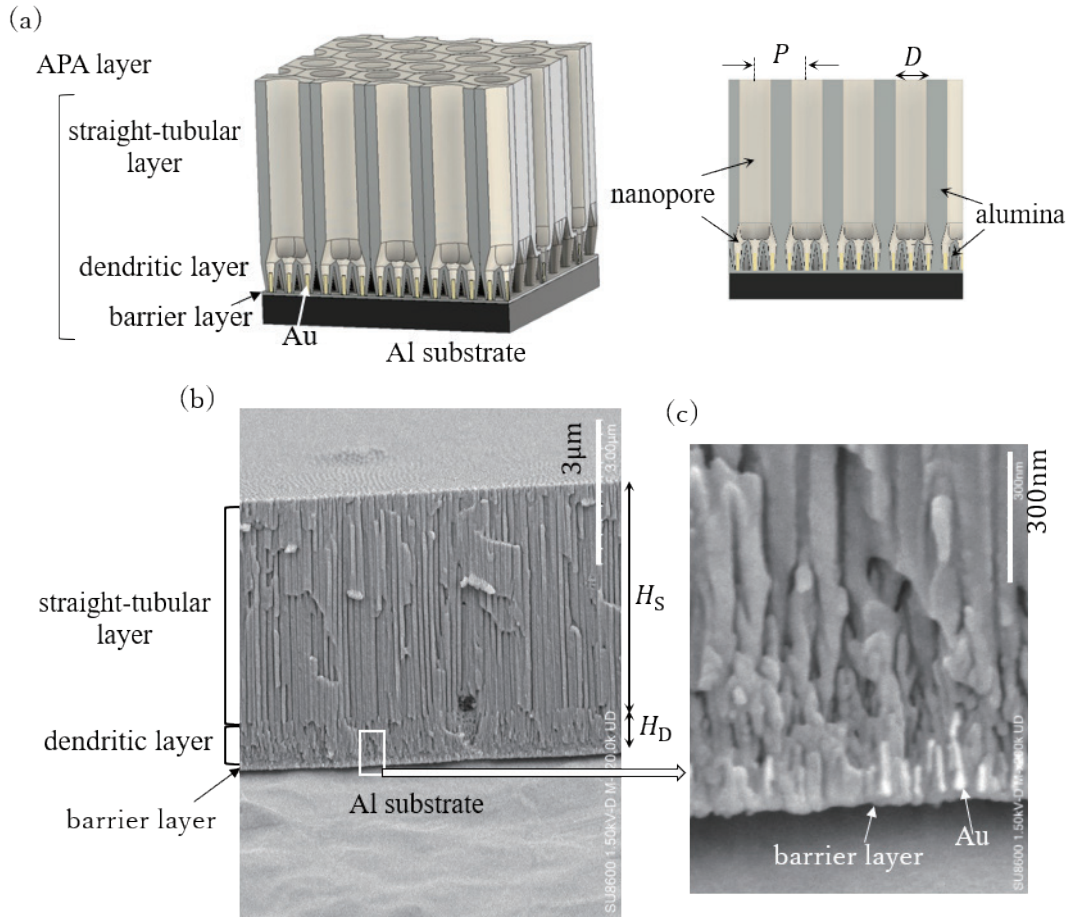

Fig. 1. (Color online) Schematic illustration of a Au-embedded APA membrane and SEM images of its cross section. Panel (a) illustrates the structure of the Au-embedded APA membrane consisting of the straight-tubular layer, the dendritic layer, and the barrier layer. Pore diameter and pore spacing are denoted by D and P, respectively. Panel (b) shows the whole view of the cross section of the Au-embedded APA membrane with E = 4.5 V. The magnification of the SEM image is 20000 times and a white bar represents 3 μm. The thickness of the straight-tubular layer is H_S = 5187 ± 103 nm and the thickness of the dendritic layer including the barrier layer is H_D = 216 ± 16 nm. Panel (c) is the enlarged view of the white rectangular area in Panel (b). The magnification of the enlarged view is 200000 times and a white bar represents 300 nm. The bright contrast in the dendritic nanopore region directly above the barrier layer indicates Au deposition.

nanopore region is formed between the bottom of a straight-tubular nanopore layer and a barrier layer on the Al substrate. Figure 1(c), which is the enlarged SEM view of the white rectangular area in Fig. 1(b), indicates the deposition of Au as bright contrast in the dendritic nanopore region directly above the barrier layer. Thus, we confirm the embedding of Au within the APA membrane by alternating current electrolysis.

3. Test Samples of Au-embedded APA Membranes

We fabricated five test samples of the Au-embedded APA membranes using different electrolysis voltages from E = 3.1 to 9 V under other electrolysis conditions fixed, i.e., a solution temperature of 25 °C and an anodization duration of 10 min. The APA membrane that has not

been embedded with Au before the electrolysis process is hereafter referred to as the bare APA membrane. The Au-embedded and bare APA membranes were cut into 1 cm squares as measurement samples. As shown in Fig. 2, the upper side of the APA layer is referred to as the top surface. Figures 2(a)–2(f) show photographs of the top surfaces of the bare APA membrane and the five Au-embedded APA membranes under daylight. The surface color of the bare APA membrane is silver-white similar to that of an Al plate, and the Au-embedded APA membrane changes its surface color from light pink to blackish purple throughout reddish pink as E increases from 3.1 to 9 V. Thus, E has a significant effect on the state of Au deposition in the APA membrane, resulting in the change of the surface color. Next, we examined the morphology and elemental composition of the Au-embedded APA membranes to estimate the state of Au deposition as E varies.

3.1 SEM observation

Figure 3 shows the top-view SEM images of the five Au-embedded APA membranes and the bare APA membrane. These images were taken by SEM (Hitachi High-Tech, SU8600, Japan). Each SEM image of the Au-embedded APA membranes indicates hexagonal nanopore arrays similar to those of the bare APA membrane. This suggests that the nanopore arrays of APA are maintained after the electrolysis process with different electrolysis voltages. Using an open source graphics software, ImageJ,[26,28] we estimated the modes (i.e., most frequently occurring values) of the pore diameter (D) and pore spacing (P) for the Au-embedded APA membranes. The D and P values for the Au-embedded APA membranes, which are indicated in the caption for each SEM image of Fig. 3, are close to those for the bare APA membrane, 67 nm and 125 nm, respectively. We also observe the distortion of the hexagonal pattern and the slight irregularities in the porous alumina, and presume some unevenness in the Au deposition. These factors can contribute to the diffuse reflection[13] that occurs along with the specular reflection when a light beam is incident on the Au-embedded APA membranes.

3.2 GD-OES analysis

We performed the elemental depth-profiling analysis of the main elements, O, Al and Au, composing the Au-embedded APA membranes by GD-OES (Horiba GD-Profiler2, Japan).[24]

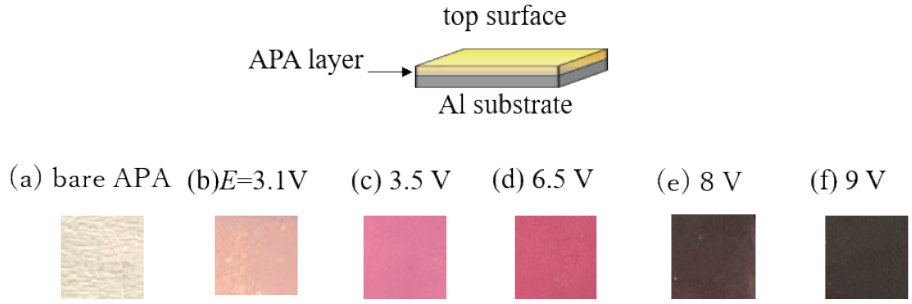

Fig. 2. (Color online) Photographs of the top surfaces of the bare APA membrane and the Au-embedded APA membranes under daylight with different electrolysis voltages from E = 3.1 to 9 V. The size of the six samples is 1 × 1 cm^2.

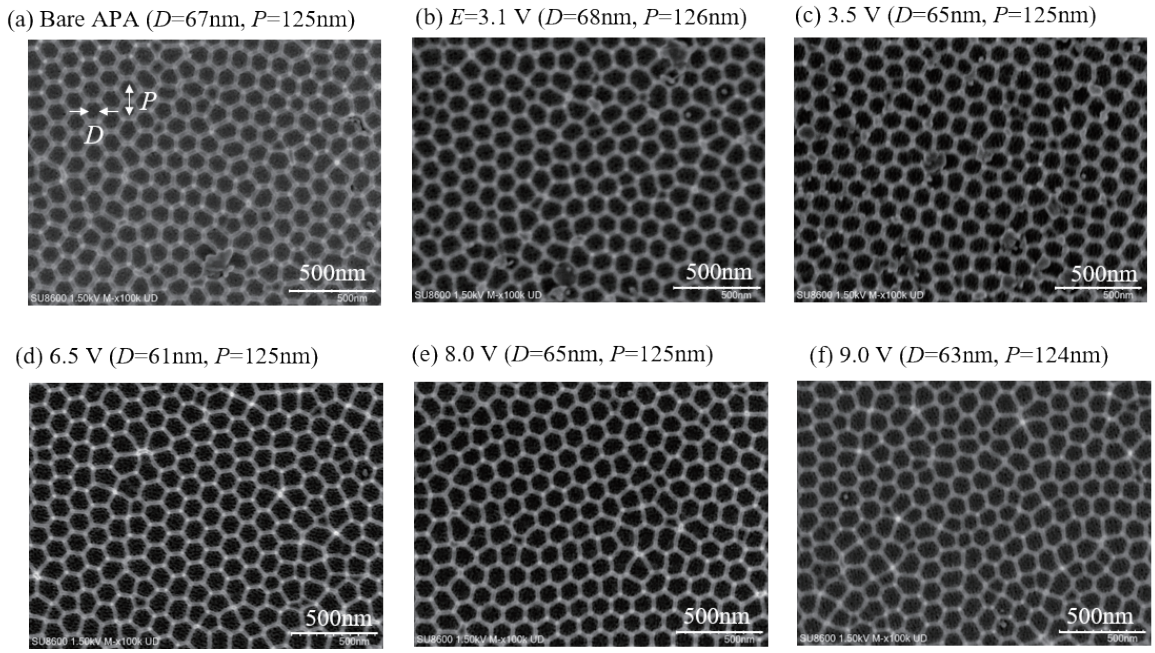

Fig. 3. Top-view SEM images for the bare APA and five Au-embedded APA membranes with different electrolysis voltages E = 3.1, 3.5, 6.5, 8.0, and 9.0 V. The pore diameter and pore spacing of each APA membrane are denoted by D and P, respectively. The magnifications of all SEM images are 100,000 times and white bars represent 500 nm.

We show the analysis results obtained by GD-OES for the bare APA membrane and the five Au-embedded APA membranes in Fig. 4, where the horizontal axis denotes the sputtering time t_s (s) (i.e., the duration required for sputter etching from the top surface of the APA layer toward the Al substrate using argon ion gas) and the vertical axis indicates the atomic ratios of the elements r_O, r_{Al}, and r_{Au} in atomic percent (at%). Figure 4(a) shows the r_O and r_{Al} curves for the bare APA membrane: the flat portions of the r_O and r_{Al} curves of t_s less than 100 s indicate the straight-tubular porous alumina layer, and the r_O curve gradually decreases to zero in the dendritic nanopore region, while the r_{Al} curve conversely increases, reaching the Al substrate. Figure 4(b), which shows the r_O, r_{Al}, and r_{Au} curves for the Au-embedded APA with E = 3.1 V, indicates the initiation of the Au deposition by electrolysis in the dendritic nanopore region. When E increases to 3.5 V [Fig. 4(c)], the r_{Au} curve rises within a certain range. This suggests that the arrays of Au nanoparticles with rod-like shapes are formed on the Al substrate side of the dendritic nanopore region in the APA membrane. The Au deposition in rod-like shapes continues up to E = 6.5 V [Fig. 4(d)]. Further increases in E allow the Au deposition to extend from the Al substrate to the bottom of the straight-tubular nanopore layer, increasing the amount of deposited Au, as indicated in Figs. 4(e) and 4(f).

As indicated in the above GD-OES analysis results, the state of Au deposition in the APA membrane depends on E: the initial state of Au deposition (E = 3.1 V); the Au deposition in the rod-like shapes (E = 3.5 to 6.5 V), and the Au deposition throughout the dendritic nanopore region (E = 8 or 9 V). We investigate the optical properties of the specular reflected light from the Au-embedded APA membrane in relation to the above three deposition states of Au.

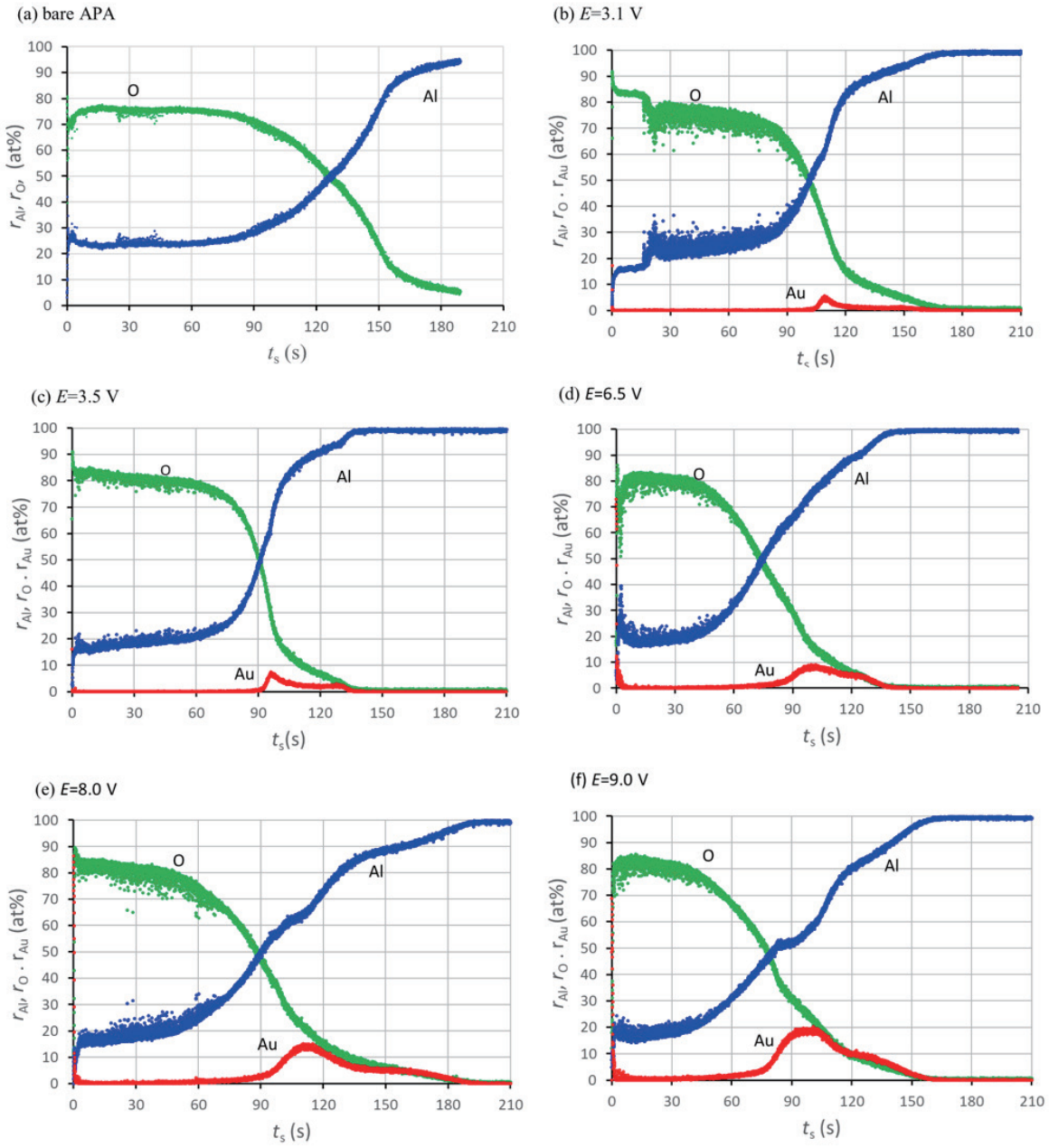

Fig. 4. (Color online) Elemental depth profiles of O, Al, and Au obtained by GD-OES for (a) the bare APA membrane and five Au-embedded APA membranes with different electrolysis voltages E = (b) 3.1, (c) 3.5, (d) 6.5, (e) 8.0, and (f) 9.0 V. The horizontal axes represent the sputtering time t_s in seconds, with the initiation of sputtering, t_s = 0 (s), corresponding to the top surface of the APA layer. The vertical axes indicate the atomic ratios of the elements r_O, r_{Al}, and r_{Au} in atomic percent.

4. Polarization Properties of Au-embedded APA Membranes

When a light beam illuminates the Au-embedded APA membranes or the bare APA membrane, a spread reflection occurs, which is a combination of specular and diffuse reflections.[13] In this study, we focus on the specular reflection light from the Au-embedded APA membranes and investigate their polarization properties.

4.1 Reflectance spectra of Au-embedded APA membranes

Before considering the polarization properties of the Au-embedded APA membranes, we examined the relative reflectance in the visible region of the specularly reflected light from them. Figure 5 shows the specular (relative) reflectance spectra of the Au-embedded APA membranes and the bare APA membrane at normal incidence. An Al mirror (Edmund Optics Japan Ltd., Stock #124, Japan) as the reference plate, a white light source (ADVATEST, TQ8111, Japan), and a multi-channel spectrometer (Ocean Optics, USB2000, USA) were used to measure the specular reflectance spectra. As shown in Fig. 5(a), the specular reflectance spectrum for the bare APA membrane indicates the oscillatory spectrum caused by the FP interference in the

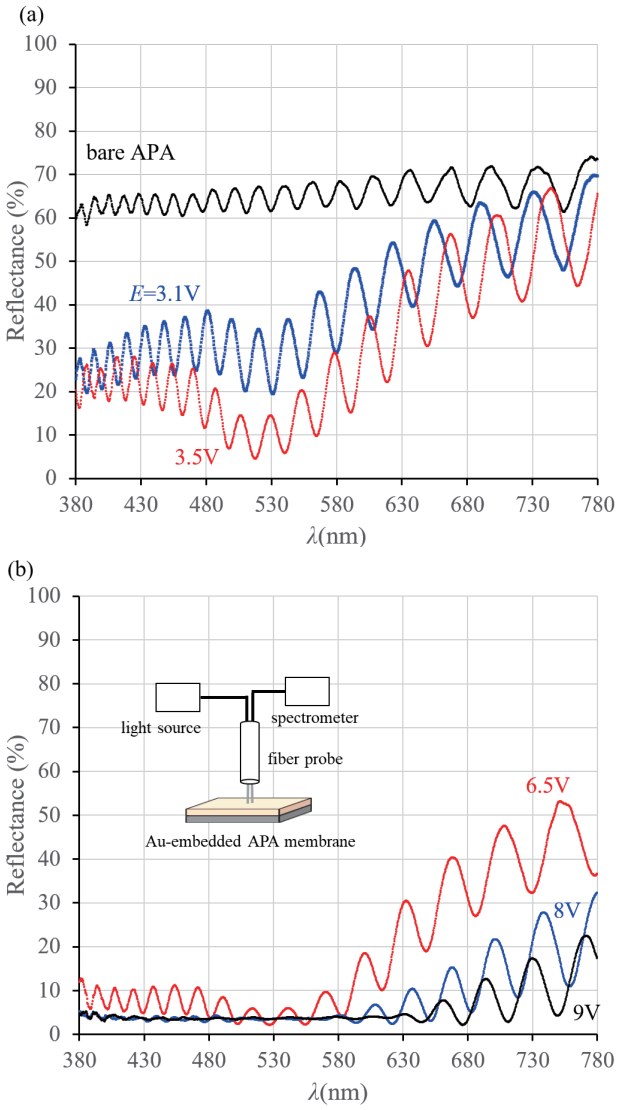

Fig. 5. (Color online) Specular reflectance spectra of the bare APA membrane and five Au-embedded APA membranes with different electrolysis voltages E: (a) bare APA membrane, E = 3.1 and 3.5 V; (b) 6.5, 8, and 9 V. The reflectance is relative to a reference Al mirror at normal incidence.

APA layer.[21] The specular reflectance spectra of the Au-embedded APA membranes change from that of the bare APA membrane as the electrolysis voltage E increases. In the specular reflectance spectrum for E = 3.1 V, a dip appears near λ = 530 nm while maintaining the oscillatory behavior due to the FP interference. When E increases to 3.5 V, the dip deepens, indicating the behavior of resonance absorption of light. Further increase in E has a large effect on the specular reflectance in the range below and around the wavelength of the dip, as indicated in Fig. 5(b). The specular reflectance spectrum for E = 6.5 V reduces the oscillatory amplitude in the range below 530 nm. As E reaches 8 V, the specular reflectance spectrum flattens in the range below 580 nm. The reflectance for E = 9 V results in an almost constant value of about 4% over the range from 420 to 620 nm.

Referring to Refs, 9, 10, and 12, we infer that the dip near λ = 530 nm of the specular reflectance spectrum of the Au-embedded APA membrane for E = 3.5 V is associated with transverse LSPs, which correspond to the surface wave mode[20] excited along the short axis of nanorods. Thus, the specular reflection near λ = 530 nm of the Au-embedded APA membrane is largely affected by the excitation of the LSPs. We hereafter investigate the polarization properties of the specularly reflected light from the Au-embedded APA membrane when the wavelength of the incident light is 532 nm. This expects an interesting polarization property to accompany both the LSP excitation and the FP interference.

4.2 Optical configuration for measurement of polarization properties

We investigate the polarization properties of the specularly reflected light from the Au-embedded APA membrane when the light of a linear polarization is incident. Figure 6 illustrates the optical configuration for the measurement of the polarization properties. The Au-embedded

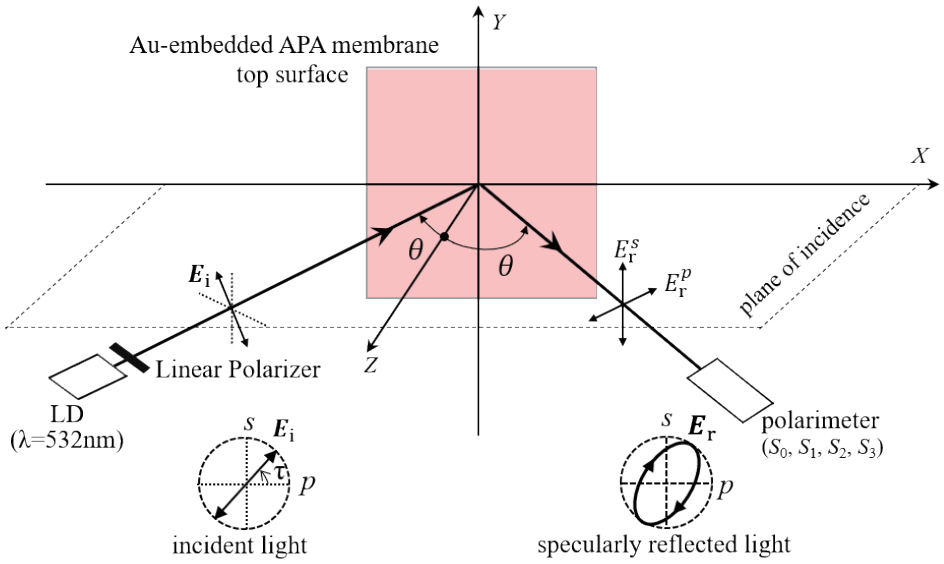

Fig. 6. (Color online) Optical configuration for measurement of polarization properties of the specularly reflected light from the Au-embedded or bare APA membrane. The linearly polarized LD light is incident on the top surface of the APA membrane.

APA membrane is located in the *XY* plane in air, and the plane of incidence is set to the *ZX* plane. We used a laser diode (LD) module (Edmund Optics Japan Ltd., Stock #37-027, Japan) as a light source. A light beam with a wavelength λ of 532 nm from the LD module illuminates the Au-embedded APA membrane at the angle of incidence θ measured from the *Z*-axis after passing through a linear polarizer (LP). The orientation of the linear polarization of the incident light is designated by the angle τ measured from the plane of incidence, and the τ values of 0 and 90° respectively represent the *p* and *s* (polarization) components. The *p* or *s* component of the light beam means that the relevant electric field is parallel or perpendicular to the plane of incidence. The intensity of the specularly reflected light from the Au-embedded APA membrane is denoted by I_r.

We measured the normalized Stokes parameters s_0 to s_3 of the specularly reflected light from the Au-embedded or bare APA membrane, using a polarimeter (Thorlabs Japan, PAX5710VIS, Japan):

$$\begin{cases} s_0\left(=\dfrac{S_0}{I_r}\right)=1 \\ s_1\left(=\dfrac{S_1}{I_r}\right)=\dfrac{1-\left(E_r^s/E_r^p\right)^2}{1+\left(E_r^s/E_r^p\right)^2} \\ s_2\left(=\dfrac{S_2}{I_r}\right)=2\dfrac{E_r^s/E_r^p}{1+\left(E_r^s/E_r^p\right)^2}\cos\delta \\ s_3\left(=\dfrac{S_3}{I_r}\right)=2\dfrac{E_r^s/E_r^p}{1+\left(E_r^s/E_r^p\right)^2}\sin\delta. \end{cases} \tag{1}$$

Here, E_r^s and E_r^p are respectively the amplitudes of the *p* and *s* components of the electric field of the specularly reflected light, and δ ($= \delta_s - \delta_p$) is the phase difference between them. The phase difference δ and the amplitude ratio E_r^s / E_r^p are evaluated from the measured Stokes parameters s_1 to s_3. We use the normalized Stokes parameter s_3, which means the difference in intensity between the right- and left-circularly polarized components and takes values from 1 (right-circular polarization) to −1 (left-circular polarization) via 0 (linear polarization).

4.3 Effects of electrolysis voltage on polarization properties

We performed the measurement of s_3 when θ is varied from 30 to 65° at τ = 15° for the bare APA membrane and each sample of the five Au-embedded membranes. Figure 7 shows the curves of s_3 obtained by the measurement. The s_3 curve for the bare APA membrane in Fig. 7(a) indicates the oscillatory behavior due to the FP interference[5,21] and remains in the negative range of s_3, or left-elliptical polarization. The s_3 curve for E = 3.1 V is similar to that of the bare APA membrane, but the magnitude of oscillation increases slightly. This slight increase is due to

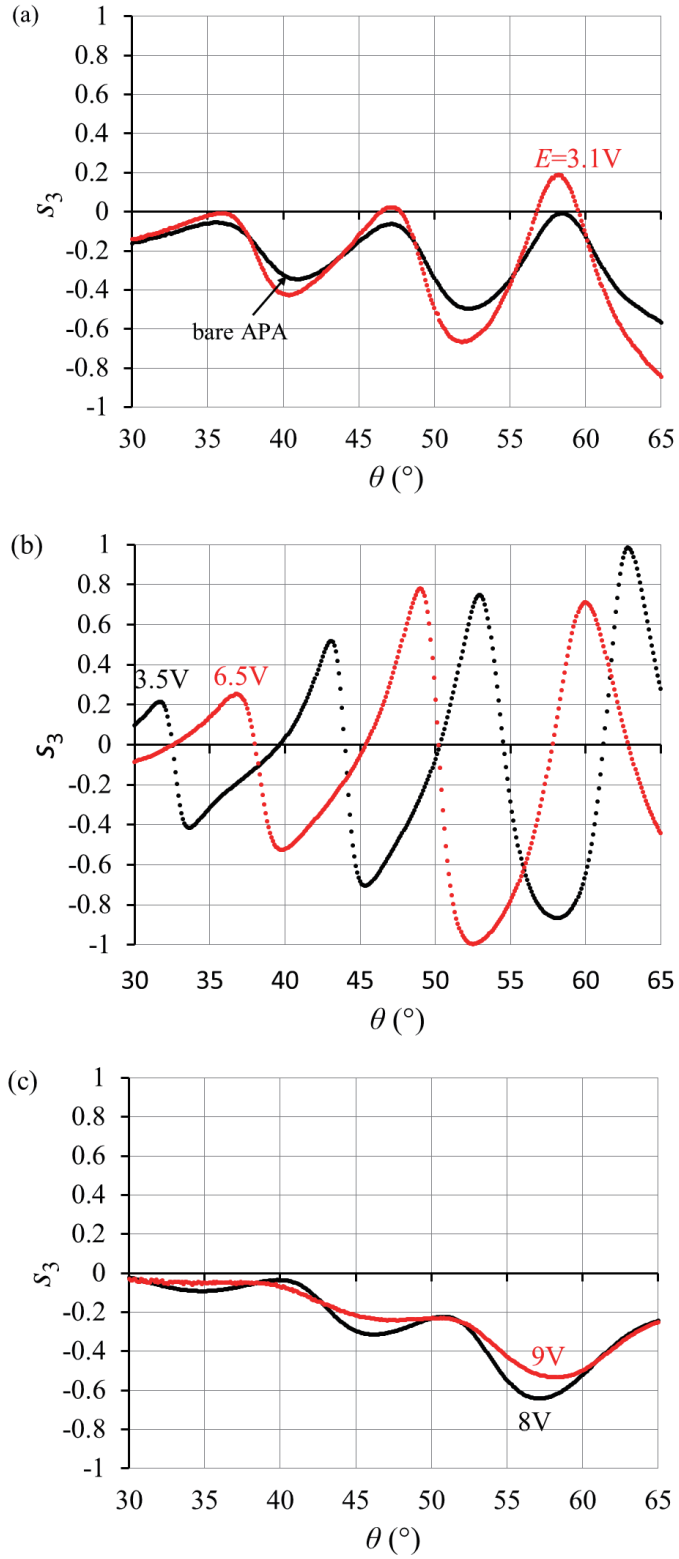

Fig. 7. (Color online) s_3 as a function of θ for specularly reflected light from the bare APA membrane and five Au-embedded APA membranes with different electrolysis voltages, under the incident light with τ = 15°: (a) bare APA and E = 3.1 V; (b) 3.5 and 6.5 V; (c) 8 and 9 V.

the initiation of the Au deposition within the APA film with $E = 3.1$ V [see the GD-OES result in Fig. 4(b)]. When E increases to 3.5 V, the oscillation amplitude of the s_3 curve becomes larger, and s_3 varies between positive and negative values, as shown in Fig. 7(b). This means that the specularly reflected light rapidly and repeatedly changes the polarization from a right- to left-ellipse, or vice versa, as θ increases. The large-amplitude oscillatory behavior in the s_3 curve, which continues up to $E = 6.5$ V, occurs in the Au-embedded APA membrane with the Au deposition in rod-like shapes [Figs. 4(c) and 4(d)]. Therefore, the large-amplitude oscillation of s_3 is closely related to the excitation of LSP on the regular arrays of Au nanoparticles with rod-like shapes inside the APA membrane. As E increases further to 8 or 9 V, where Au is widely and much deposited throughout the dendritic nanopore region of the APA layer [Figs. 4(e) and 4(f)], the s_3 curve remains in the negative range of s_3, reducing the oscillation amplitude, as shown in Fig. 7(c).

As stated above, the incident-angle dependence of s_3 in the specularly reflected light from the Au-embedded APA membrane can be roughly classified into three types according to E. We examine the three types of the θ dependence of s_3 in detail through the behaviors of the phase difference δ and the amplitude ratio E_r^s / E_r^p of the p and s components of the specularly reflected light, which are quantities that determine the state of polarization. Figure 8 shows s_3, δ, and E_r^s / E_r^p as functions of θ for the Au-embedded APA membranes with $E = 3.1$, 3.5, and 8 V under the incident light with $\tau = 15°$. When E is 3.1 V, the δ curve oscillates between 150 and 300° and the E_r^s / E_r^p curve exhibits alternating local minimum and maximum at equal θ intervals. These behaviors of the δ and E_r^s / E_r^p curves are associated with the FP interference in the APA layer, resulting in the s_3 curve oscillating in the negative range. On the other hand, the δ curve for $E = 3.5$ V exhibits a marked variation ranging continuously from around 180 to −720°, whereas the E_r^s / E_r^p curve exhibits a trend similar to that observed for $E = 3.1$ V. As a result, the s_3 curve for $E = 3.5$ V oscillates in a positive to negative range, increasing the amplitude with an increase in θ. Note that the continuous and large-range variation in δ is caused by the presence of the arrays of Au nanoparticles with rod-like shapes inside the APA membrane. Consequently, we clarify that the large-amplitude oscillatory behavior in the s_3 curve is attributed to the simultaneous occurrence of the FP interference and LSP excitation. When E reaches 8 V, the δ curve increases around 180° while oscillating slightly, and the E_r^s / E_r^p curve differs from those of $E = 3.1$ and 3.5 V. Therefore, the s_3 curve for $E = 8$ V exhibits the oscillatory behavior with a reduced amplitude in the negative range of s_3.

As the E_r^s / E_r^p of the specularly reflected light is affected by the orientation of the linear polarization of the incident light τ, we examined the θ dependence of s_3 for different τ values. Figure 9 shows s_3, δ, and E_r^s / E_r^p as functions of θ for $\tau = 10$, 20, and 30° of the specularly reflected light from the Au-embedded APA membrane with $E = 3.5$ V. As can be seen from Figs. 9(b) and 9(c), τ does not affect the δ curve, but the E_r^s / E_r^p curve shifts vertically with a variation in τ. If we choose τ such that E_r^s / E_r^p is close to unity at θ corresponding to $\delta = 90$ or −90°, then s_3 approaches +1 or −1, as expected from Eq. (1). Indeed, $s_3 = -1$ [point A in Fig. 9(a)] at $\theta = 44.9°$ in the s_3 curve for $\tau = 30°$ is given by $\delta = -90.3°$ [A_1 in Fig. 9(b)] and $E_r^s / E_r^p = 0.97$ [A_2 in Fig. 9(c)]. Similarly, $s_3 = 1$ [point B in Fig. 9(a)] at $\theta = 53.1°$ in the s_3 curve for $\tau = 30°$ is due to $\delta = -271.6°$ (~88.4°) [B_1 in Fig. 9(b)] and $E_r^s / E_r^p = 1.08$ [B_2 in Fig. 9(c)]. Thus, setting τ to 30°

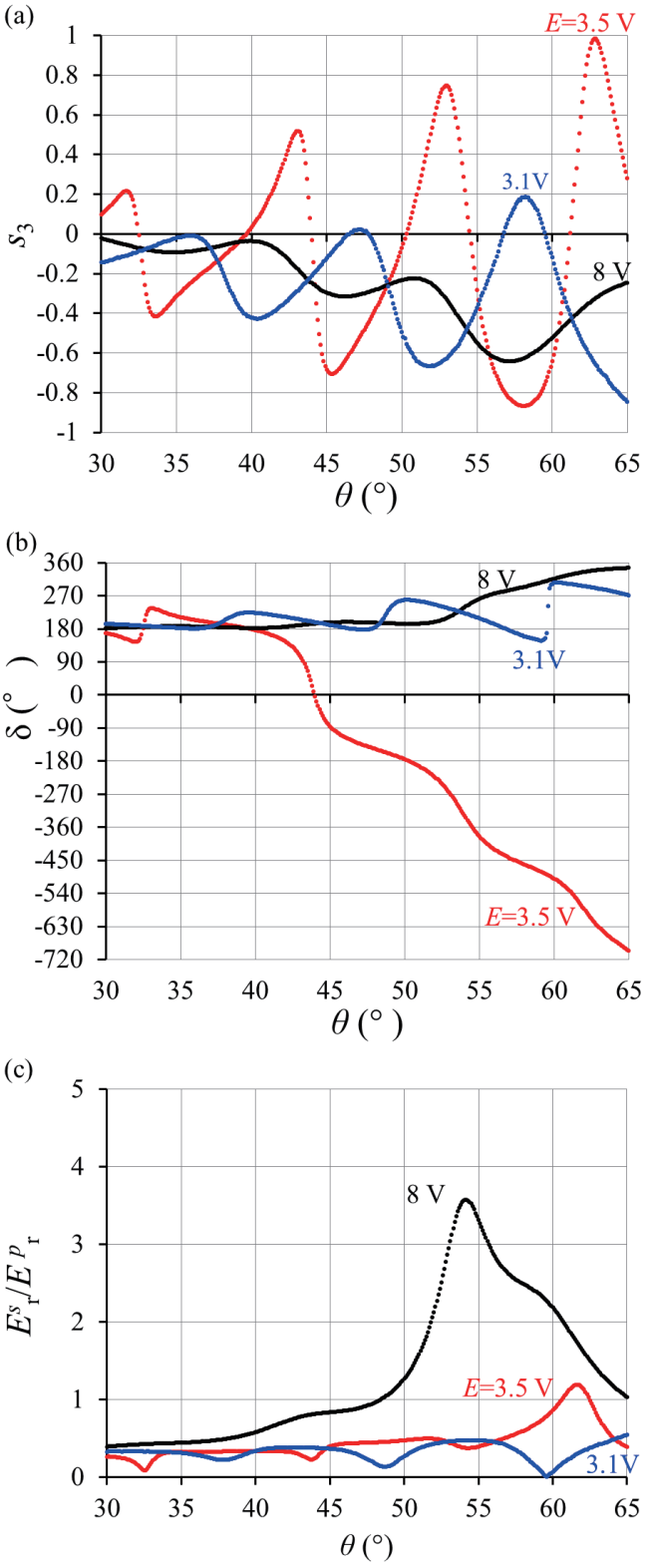

Fig. 8. (Color online) s_3, δ, and E_r^s/E_r^p as functions of θ for the Au-embedded APA membranes with E = 3.1, 3.5, and 3.5 V under incident light with τ = 15°.

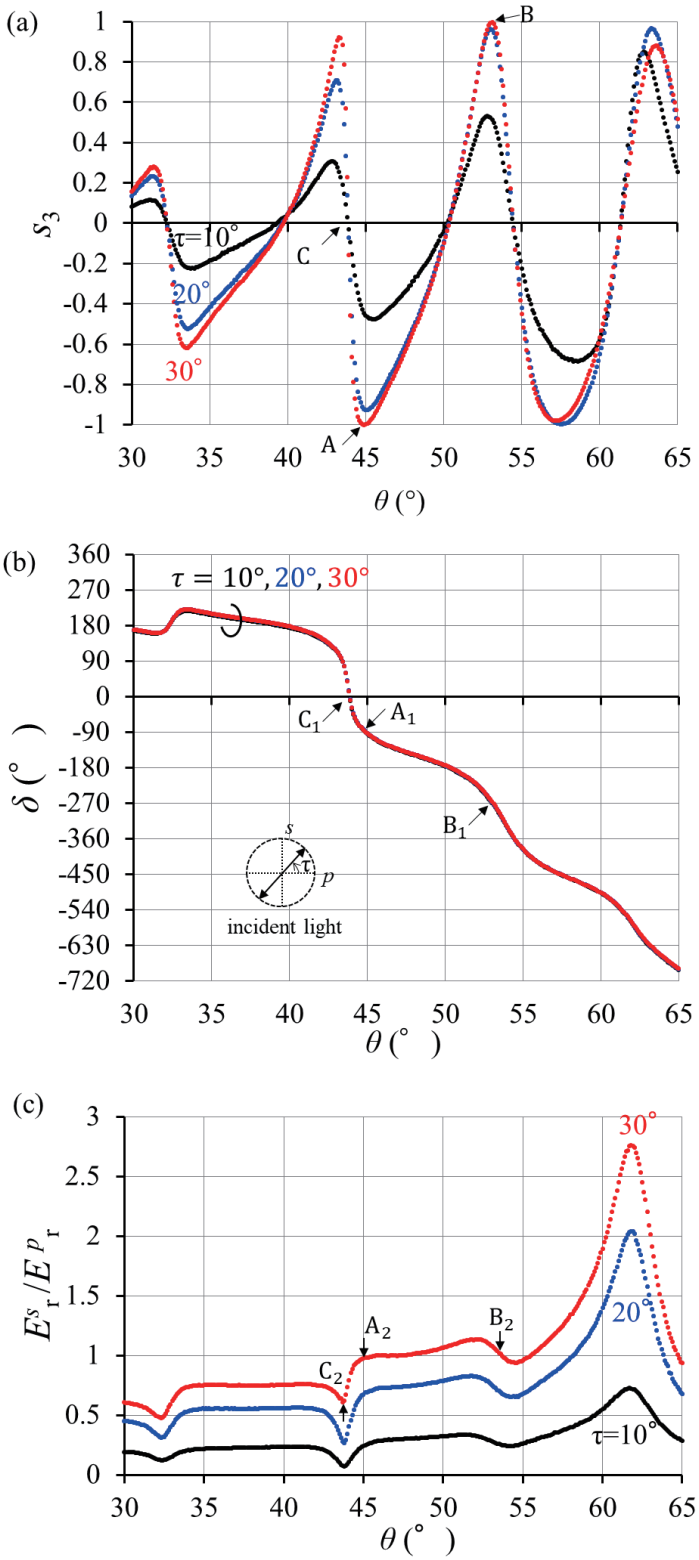

Fig. 9. (Color online) s_3, δ, and E_r^s/E_r^p as functions of θ for τ = 10, 20, and 30° in the Au-embedded APA membrane with E = 3.5 V.

enables s_3 to vary rapidly and throughout the entire range from −1 to +1. Furthermore, we observe that the s_3 curve for $\tau = 30°$ has a steep slope at the zero-crossing point of $\theta = 43.8°$ [C in Fig. 9(a)]. The steep slope is caused by the rapid shift in δ [C_1 in Figs. 9(b)] and the sharp dip in E_r^s / E_r^p [C_2 in Fig. 9(c)], which are considered to be due to the simultaneous occurrence of the FP interference in the APA layer and the LSP excitation on the arrays of Au nanoparticles. Thus, s_3 near the zero-crossing point is expected to be highly sensitive to variations in the structural parameters of the Au-embedded APA membrane, including the dimension of Au rod-like nanoparticles and the refractive index of materials filling the straight tubular nanopores.

4.4 Effective medium approximation for the Au-embedded APA membrane

In Sect. 4.3, we experimentally showed the rapid change in the s_3 of the specularly reflected light from the Au-embedded APA membrane. This rapid change can be attributed to the simultaneous occurrence of the FP resonance in the APA layer and the LSP excitation on the arrays of Au rod-like nanoparticles. Here, we roughly examine the rapid change in s_3 from numerical aspects based on the Maxwell Garnett theory,[29] which has been commonly used for the EM approximation of porous alumin.[9,10] As illustrated in Fig. 10(a), we approximate the Au-embedded APA membrane as the three-layer structure consisting of the straight-tubular (nanopore) layer, the dendritic (nanopore) layer, and the Al substrate. The straight-tubular layer is expressed by the ordered hexagonal arrays of nanopores of air-filled cylinders. The diameter and spacing of the cylinders are denoted by D_1 and P_1, respectively, and their length is H_S. The dendritic layer is approximated by the ordered hexagonal arrays of cylindrical nanopores in which the lower portion of length H_{Au} is filled with Au and the upper portion of length H_D is air. The diameter and spacing of the cylindrical nanopores are denoted by D_2 and P_2, respectively. The barrier layer between the dendritic region and the Al substrate is not taken into account in the numerical simulation owing to its very small thickness.

Since the sizes of the nanopores in the straight-tubular and dendritic layers are much smaller than the wavelength of the incident light, the Maxwell Garnett EM approximation is performed for the porous media. As a result, the Au-embedded APA membrane is modeled as a

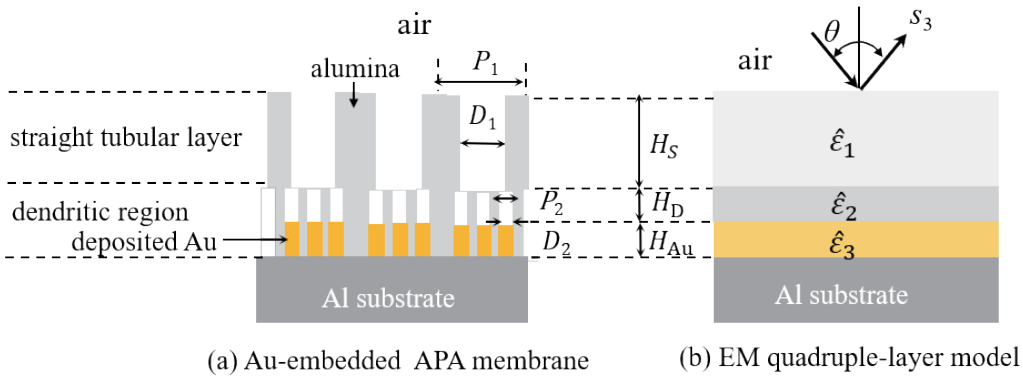

Fig. 10. (Color online) EM quadruple-layer model for the Au-embedded APA membrane based on the Maxwell Garnet EM approximation. The structural parameters used for the EM quadruple-layer model are $D_1 = 65$ nm, $P_1 = 125$ nm, $H_S = 5200$ nm, $D_2 = 22$ nm, $P_2 = 63$ nm, $H_D = 100$ nm, and $H_{Au} = 120$ nm.

homogeneous quadruple-layer structure [as illustrated in Fig. 10(b)], which is hereinafter referred to as the EM quadruple-layer model. The effective dielectric constants of the top and second layers in the model are given by

$$\hat{\varepsilon}_j = \varepsilon_{\mathrm{Al_2O_3}} \frac{\left(1+2f_j\right)\varepsilon_{pore} + 2\left(1-f_j\right)\varepsilon_{\mathrm{Al_2O_3}}}{\left(1-f_j\right)\varepsilon_{pore} + \left(2+f_j\right)\varepsilon_{\mathrm{Al_2O_3}}} \quad \left(j=1,2\right). \tag{2}$$

Here, $\varepsilon_{\mathrm{Al_2O_3}}$ and ε_{pore} are respectively the dielectric constants of Al_2O_3 and pore-filling material (or air), and $f_j = \frac{\pi}{2\sqrt{3}}\left(\frac{D_j}{P_j}\right)^2$ is the volume fraction of pores in the straight-tubular layer (j = 1) or the dendritic layer (j = 2). The effective dielectric constant of the third layer, which corresponds to the layer of the Au nanoparticle arrays inside the dendritic layer, is approximated by

$$\hat{\varepsilon}_3 = \varepsilon_{\mathrm{Al_2O_3}} \frac{\left(1+2f_2\right)\varepsilon_{\mathrm{Au}} + 2\left(1-f_2\right)\varepsilon_{\mathrm{Al_2O_3}}}{\left(1-f_2\right)\varepsilon_{\mathrm{Au}} + \left(2+f_2\right)\varepsilon_{\mathrm{Al_2O_3}}}, \tag{3}$$

where $\varepsilon_{\mathrm{Au}}$ is the complex dielectric constant of Au. Although the EM approximate medium for Au-nanoparticle arrays needs to be considered as an anisotropic medium,[9,10] we here treat it as an isotropic medium for simplicity.

The reflection problem of plane waves from the EM quadruple-layer model is numerically solved by the transfer matrix method (TMM).[30] The structure parameters used for the numerical computation are determined with reference to the SEM images in Figs. 1 and 3: D_1 = 65 nm, P_1 = 125 nm, and H_S = 5200 nm; D_2 = 22 nm, P_2 = 63 nm, H_D = 100 nm, and H_{Au} = 120 nm. The refractive indices of Al_2O_3, Au, and Al are obtained from an online database.[31] The refractive indices at λ = 532 nm are $n_{\mathrm{Al_2O_3}}$ =1.7718, n_{Au} = 0.54386 − j2.2309, and n_{Al} = 0.93878 − j6.4195. The refractive index of the pore filling material (or air) is n_{pore} = 1.0003. Figure 11 shows the numerical results of the specular reflectance spectrum and s_3 as functions of θ obtained using the EM quadruple-layer model, together with the corresponding experimental data for the Au-embedded APA membrane with E = 3.5 V. Similarly to the experimental data in Fig. 5(a), the numerical results exhibit oscillatory behavior and a dip near λ = 530 nm in the specular reflectance spectrum. The polarization property of the numerical results indicates the rapid change in s_3, which is similar to the experimental data in Fig. 7(b). As described above, the EM quadruple-layer model approximates the optical properties of the Au-embedded APA membrane with E = 3.5 V to exhibit the occurrence of the FP interference and LSP excitation.

4.5 Discussion

We have experimentally investigated the polarization properties of the specularly reflected light from the Au-embedded APA membranes, in which various states of Au deposition were formed by tuning the electrolysis voltage in alternating current electrolysis. As a result, we

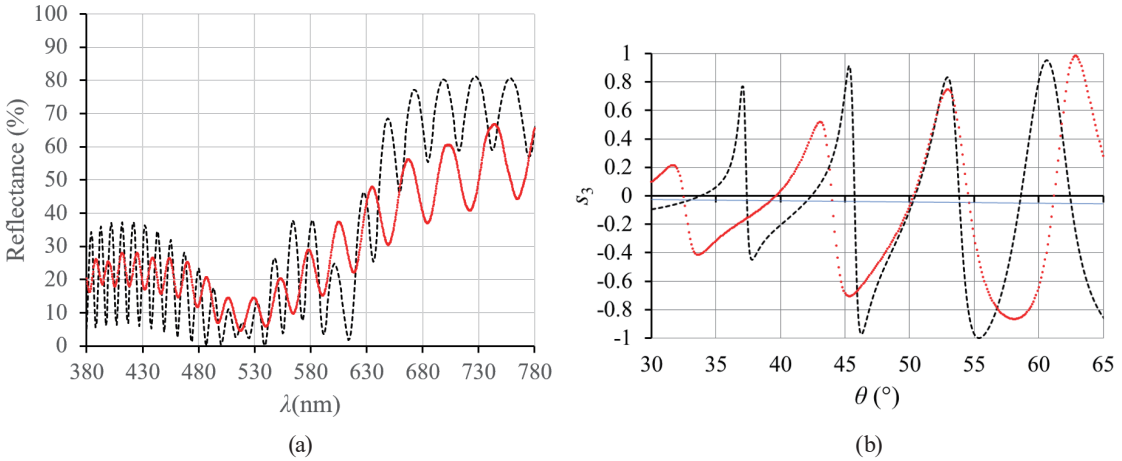

Fig. 11. (Color online) Numerical results of the EM quadruple-layer model (broken lines) and the experimental data (dotted curves) for the Au-embedded APA membrane with E = 3.5 V. The experimental data are those in Figs. 5(a) and 7(b). (a) Specular reflectance spectrum at normal incidence; (b) s_3 as a function of θ at λ = 532 nm.

revealed that, when the Au-embedded APA membrane is considered to have the Au rod-like nanoparticle arrays, the specularly reflected light changes rapidly from right- to left-circular polarization via linear polarization, or vice versa, with a slight variation in the angle of incidence of the 532 nm light. The rapid change in s_3 is explained by the behavior of the phase difference (δ) between the p and s components of the specularly reflected light: the excitation of the transverse LSPs increases the variation in δ that occurs through the FP interference, resulting in the rapid change in s_3. The numerical simulation based on the Maxwell Garnett EM approximation also indicates the rapid change in s_3 in the Au-embedded APA membrane. Consequently, we consider that the rapid change in s_3 is the result of the simultaneous occurrence of the FP interference in the APA layer and the LSP excitation on the rod-like nanoparticle arrays.

The rapid change in s_3 occurring in the Au-embedded APA membrane requires further investigation. The deposition of Au into the APA film was confirmed by the analytical results of GD-OES for the Au-embedded APA membrane. However, the size and shape of the Au-deposited particles have not yet been identified. To determine the structural parameters, it is necessary to make precise observations of the cross section of the Au-embedded APA membrane. Subsequent to determining the structure and constituent materials of the Au-embedded APA membrane, a more rigorous numerical simulation can be performed to investigate its optical properties in detail. The numerical simulation enables us to theoretically demonstrate the occurrence mechanism of the rapid change in s_3. Furthermore, the numerical simulation facilitates our clear understanding of the effects of the structural parameters of the Au-embedded APA membrane on the polarization properties of the specular reflected light.

Although we have investigated the optical properties of the specularly reflected light from the Au-embedded APA membrane, the examination of diffuse reflection is also a topic of interest.[13] Some unevenness in the deposition of Au into nanopores may contribute to the diffuse reflection, together with the distortion of the hexagonal pattern or the slight irregularities in the surface of

porous alumina. The Au deposition within the APA membrane is expected to affect optical qualities of color such as chromaticity and glossiness, which are characterized by a diffuse reflection.

5. Conclusion

We have fabricated a Au-embedded APA membrane through two-step anodization followed by alternating current electrolysis. The Au-embedded APA membrane exhibits an interesting polarization property that s_3 changes rapidly and largely with respect to the slight variation in the angle of incidence of the LD light with a wavelength near 532 nm. The rapid change in s_3 can be highly dependent on the structure and composition of the Au-embedded APA membrane.[32] This suggests the potential for a novel utilization of the Au-embedded APA membrane in polarization-based devices. For instance, the rapid variation in the zero-crossing point of the s_3 curve may be used to detect small changes in the refractive index of the specimen in the nanopores of APA, as biosensors or chemical sensors.[6,33] The Au-embedded APA membrane can be also interesting from a practical point of view owing to its simple, cost-effective, and large-area fabrication process.

Acknowledgments

This work was partially supported by the Association for Regional Cooperation and Promotion with National Institute of Technology, Kumamoto College. The authors would like to thank Mr. Kunihiko Miyazaki (Kumabou Metal Co., Ltd.) and Dr. Yoshiro Ohgi (Kumamoto Industrial Research Institute) for their valuable technical assistance in the compositional and morphological analyses of the Au-embedded APA membrane.

References

1 W. Lee and S.-J. Park: Chem. Rev. **114** (2014) 7487. https://doi.org/10.1021/cr500002z
2 J. T. Domagalski, E. Xifre-Perez, and L. F. Marsal: Nanomaterials **11** (2021) 430. https://doi.org/10.3390/nano11020430
3 H. Masuda and K. Fukuda: Science **268** (1995) 1466. https://doi.org/10.1126/science.268.5216.1466
4 H. Masuda and K. Nishio: Self-Organized Nanoscale Materials, M. Adachi and D. J. Lockwood, Eds. (Springer-Verlag, New York, 2006) Chap. 9. https://link.springer.com/chapter/10.1007/0-387-27976-8_9
5 K. S. Choudhari, C.-H. Choi, S. Chidangil, and S. D. George: Nanomaterials **12** (2022) 444. https://doi.org/10.3390/nano12030444
6 M. A. Tabrizi, J. Ferre-Borrull, and L. F. Marsal: Sensors **20** (2020) 5068. https://doi.org/10.3390/s20185068
7 A. Ruiz-Clavijo, O. Caballero-Calero, and M. Martín-González: Nanoscale **13** (2021) 2227. https://doi.org/10.1039/D0NR07582E
8 C. A. Foss Jr., G. L. Hornyak, J. A. Stockert, and C. R. Martin: J. Phys. Chem. **98** (1994) 2963. https://doi.org/10.1021/j100062a037
9 B. G. McMillan, L. E. A. Berlouis, F. R. Cruickshank, D. Pugh, and P.-F. Brevet: Appl. Phys. Lett. **86** (2005) 211912. https://doi.org/10.1063/1.1939070
10 R. Atkinson, W. R. Hendren, G. A. Wurtz, W. Dickson, A. V. Zayats, P. Evans, and R. J. Pollard: Phys. Rev. B **73** (2006) 235402. https://doi.org/10.1103/PhysRevB.73.235402
11 N. Taşaltın, S. Öztürk, N. Kılınç¸ H. Yüzer, and Z. Z. Öztürk,: Nanoscale Res. Lett. **5** (2010) 1137. https://doi.org/10.1007/s11671-010-9616-z
12 M. Shaban, H. Hamdy, F. Shahin, and S.-W. Ryu: J. Nanosci. Nanotechnol. **10** (2010) 3034. https://doi.org/10.1166/jnn.2010.2180

13 A. Yasui, T. Kawahara, M. Iwasaki, S. Karuppuchamy, H. Tada, and S. Ito: J. Jpn. Soc. Colour Mater. **79** (2006) 190. https://doi.org/10.4011/shikizai1937.79.190
14 X. Hu, Y. J. Pu, Z. Y. Ling, and Y. Li: Opt. Mater. **32** (2009) 382. https://doi.org/10.1016/j.optmat.2009.09.009
15 T. Kumeria, A. Santos, and D. Losic: Sensors **14** (2014) 11878. https://doi.org/10.3390/s140711878
16 Y. Tomaru, T. Tani, Y. Hotta, Y. Hatanaka, and M. Naya: Fujifilm Res. Dev. **53** (2008) 36. https://asset.fujifilm.com/www/jp/files/2020-01/c66ba036f10007be5db6630fd19bed13/ff_rd053_all_en.pdf
17 C.-Y. Liu, R. Ram, R. B. Kolaru, A. S. Jana, A. S. Sadhu, C.-S. Chu, Y.-N. Lin, B. N. Pal, S.-H. Chang, and S. Biring: Biosensors **12** (2022) 807. https://doi.org/10.3390/bios12100807
18 K.-H. Kim, E. Lefeveure, M. Châtelet, and C.-S. Cojocaru: MRS Online Proc. Lib. **1439** (2012) 11. https://doi.org/10.1557/opl.2012.940
19 A. Akouibaa, R. Masrour, A. Jabar,·M. Benhamou, M. Ouarch, and A. Derouiche: Plasmonics **17** (2022) 1157. https://doi.org/10.1007/s11468-022-01607-w
20 C. F. Bohren and D. R. Huffman: Absorption and Scattering of Light by Small Particles (WILEY-VCH Verlag GmbH & Co. KGaA, Weiheim, 1998) Chap. 12. https://doi.org/10.1002/9783527618156.ch3
21 A. Santos, V. S Balderrama, M. Alba, P. Formentín, J. Ferré-Borrull, J. Pallarès, and L. F Marsal: Nanoscale Res. Lett. **7** (2012) 370. https://doi.org/10.1186/1556-276X-7-370
22 K. S. Napolskii, I. V. Roslyakov, A. A. Eliseev, D. I. Petukhov, A. V. Lukashin, S.-F. Chen, C.-P. Liu, and G. A. Tsirlina: Electrochim. Acta **56** (2011) 2378. https://doi.org/10.1016/j.electacta.2010.12.013
23 G. A. Gelves, B. Lin, U. Sundararaj, and J. A. Haber: Adv. Funct. Mater. **16** (2006) 2423. https://doi.org/10.1002/adfm.200600336
24 M. Iwai and T. Kikuchi: Electrochim. Acta **399** (2021) 139440. https://doi.org/10.1016/j.electacta.2021.139440
25 C. T. Sousa, D. C. Leitão, M. P. Proença, A. Apolinário, J. G. Correia, J. Ventura, and J. P. Araújo: Nanotechnology **22** (2011) 315602. https://doi.org/10.1088/0957-4484/22/31/315602
26 L. Sacco, I. Florea, and C.-S. Cojocaru: Surf. Coat. Technol. **364** (2019) 248. https://doi.org/10.1016/j.surfcoat.2019.02.086
27 A. Yadav, M. Muthukumar, and M. S. Bobji: Surf. Interfaces **24** (2021) 101115. https://doi.org/10.1016/j.surfin.2021.101115
28 ImageJ: https://imagej.net/ij/ (accessed April 2025).
29 J. C. M. Garnett: Philos. Trans. R. Soc. London Ser. A **203** (1904) 385. https://doi.org/10.1098/rsta.1904.0024
30 E. Hecht: Optics (Addison Wesley, San Francisco, 2002) 4th ed., Chap. 4.
31 RefractiveIndex.INFO - Refractive index database: https://refractiveindex.info/ (accessed September 2025).
32 T. Matsuda, I. Tsunoda, M. Nagata, T. Kawakita, and S. Noguchi: Appl. Opt. **61** (2022) 10178. https://doi.org/10.1364/AO.474161
33 G. Sriram, P. Patil, M. P. Bhat, R. M. Hegde, K. V. Ajeya, I. Udachyan, M. B. Bhavya, M. G. Gatti, U. T. Uthappa, G. M. Neelgund, H.-Y. Jung, T. Altalhi, Madhuprasad, and M. D. Kurkuri: J. Nanomater. **2016** (2022) 1753574. https://doi.org/10.1155/2016/1753574